Journal of Power Sources 273 (2015) 465–471

Contents lists available at ScienceDirect

Journal of Power Sources

journal homepage: www.elsevier.com/locate/jpowsour

# Green fabrication of composite cathode with attractive performance for solid oxide fuel cells through facile inkjet printing

Chao Li [a], Huili Chen [b, c], Huangang Shi [a], Moses O. Tade [b], Zongping Shao [a, b, *]

[a] State Key Laboratory of Materials-Oriented Chemical Engineering, Nanjing Tech University, Nanjing 210009, China
[b] Department of Chemical Engineering, Curtin University, Perth, WA 6458, Australia
[c] The Institute of Molecular Science, Shanxi University, Taiyuan 030006, China

## HIGHLIGHTS

- The cathode layer was fabricated by inkjet printing.
- The cathode layer was based on environmentally friendly water-based ink.
- A pore former was introduced into the cathode ink.
- High power and OCV were obtained for the cell with cathode preparation by inkjet printing.

## ARTICLE INFO

*Article history:*
Received 30 July 2014
Received in revised form
28 August 2014
Accepted 22 September 2014
Available online 30 September 2014

*Keywords:*
Inkjet printing
Solid oxide fuel cells
Cathode
Thin layer
Fabrication

## ABSTRACT

The inkjet printing technique has numerous advantages and is attractive in solid oxide fuel cell (SOFC) fabrication, especially for the dense thin electrolyte layer because of its ultrafine powder size. In this study, we exploited the technique for the fabrication of a porous SDC/SSC composite cathode layer using environmentally friendly water-based ink. An optimized powder synthesis method was applied to the preparation of the well-dispersed suspension. In view of the easy sintering of the thin film layer prepared by inkjet printing, 10 wt.% pore former was introduced to the ink. The results indicate that the cell with the inkjet printing cathode layer exhibits a fantastic electrochemical performance, with a PPD as high as 940 mW $cm^{-2}$ at 750 °C, which is comparable to that of a cell prepared using the conventional wet powder spraying method, suggesting a promising application of inkjet printing on electrode layer fabrication.



## 1. Introduction

Innovative technologies that can lead to increased efficiency and reduced impact on environment during energy utilization are always important for a sustainable development of our society. Fuel cells are an innovative technology that are reputed for their high energy conversion efficiency up to 80% and low emissions with a reduction in $CO_2$ emission of approximately 50% per kW of electricity compared with traditional power generation based on combustion engines [1–4]. A combination of solid-oxide fuel cells (SOFCs), high-temperature electrochemical energy conversion devices, with renewable biofuels, may provide a practical solution for providing clean electric power supply of the future [5–7].

The fabrication cost, material cost, cell power output, and cell lifetime are some of the important factors that largely determine the practical application of SOFC technology. Currently, the research trend on SOFCs is shifted to reduce the operation temperature from approximately 1000 °C to the range of 500–800 °C [8–19], because such a reduction could lead to prolonged cell lifetime and reduced materials cost. To obtain a high cell power output, a thin-film electrolyte configuration is often adopted in intermediate temperature (IT)-SOFCs to offset the decrease in ionic conductivity with a decrease of operation temperature [20–23]. When tape casting has been demonstrated to be a cost-effective technique for the mass production of thick anode substrates, an anode is typically selected as the substrate [24–26]. Therefore, the development of methods for economic fabrication of thin film electrolytes and cathodes becomes one of the critical points in achieving the practical application of IT-SOFCs.

* Corresponding author. State Key Laboratory of Materials-Oriented Chemical Engineering, Nanjing Tech University, Nanjing 210009, China. Tel.: +86 25 83172256; fax: +86 25 83172242.
*E-mail addresses:* shaozp@njtech.edu.cn, shaozp@njut.edu.cn (Z. Shao).

http://dx.doi.org/10.1016/j.jpowsour.2014.09.143
0378-7753/

Inkjet printing is a highly attractive technique for the deposition of thin layers in a wide range of areas including electronics processing, fine ceramics, and biological culture research [27–33]. Very recently, the application of the inkjet printing technique in the fabrication of SOFCs was also well noted [34–42], as this technique has several important advantages. First, inkjet printing can be fully automated, providing easy mass production; second, the film pattern, such as the size and thickness, can be precisely controlled, ensuring high production reproducibility; third, the fabrication is non-contact without the requirement of a mask or screen, providing non-destructive fabrication.

There have been several publications available in the literature on the fabrication of SOFCs by inkjet printing to date [34–42]; however, most of the successful attempts were focused on the dense thin-film electrolyte or thin functional layers [34–39], while few reports are available on porous electrodes [40–42]. Typically, the cathode prepared by inkjet printing performed worse than that prepared by conventional slurry painting [41]. For example, Yashiro et al. attempted to fabricate a LSCF-GDC cathode using inkjet printing method using a water-based slurry and observed that the as-prepared cathode layer had a graded size distribution with respect to depth due to the effect of gravity and caused the formation of a dense surface layer, which resulted in poor gas permeation and then poor electrode performance [41]. To improve the cathode performance, an additional slurry painted layer was required [41]. However, the double-layered cathode configuration increased the fabrication cost.

Sukeshini et al. comparatively studied the anode-supported SOFCs with cathode prepared using a slurry paste and inkjet printing [40]. α-terpineol was applied as an organic solvent, and polyvinylbutyral (PVB) and butyl benzyl phthalate (BBP) and polyalkalyne glycol (PAG) were utilized as the binder and plasticizer constituents. These researchers demonstrated that the microstructure of the printed layers could be tailored by altering the rheological property of the ink and/or the printing process parameters. After optimization, the cells could deliver similar performance with the cathode prepared by hand painting. Compared with organic solvent-based inks, water-based inks are more environmentally friendly, and thus much more attractive for practical applications.

In this study, we report our exploitation on the fabrication of a porous cathode layer by inkjet printing using environmentally friendly water-based ink. A $Sm_{0.5}Sr_{0.5}CoO_3$ (SSC) + $Sm_{0.2}Ce_{0.8}O_{1.9}$ (SDC) composite cathode was used. For the easy sintering of the thin film layer prepared by inkjet printing because of the ultrafine powder size, the use of a pore former was also attempted. We demonstrated that both the pore former and powder loading in the ink are important to the microstructure and, consequently, the performance of the electrode. After optimization, the as-prepared composite electrode delivered comparable performance to that achieved by spray deposition, which is highly promising for its practical application in SOFCs.

## 2. Experimental

### 2.1. Cathode powder synthesis

The SSC powder was synthesized by a combined EDTA-citrate sol–gel method, while the SDC powder was synthesized using a hydrothermal process. All the related raw materials mentioned below were purchased from Sinopharm Chemical Reagent Co. Ltd., Shanghai, China in analytical grade. For SSC, a stoichiometric amount of $Sm(NO_3)_3 \cdot 6H_2O$, $Sr(NO_3)_2$, and $Co(NO_3)_2 \cdot 6H_2O$ were mixed with the molar ratio of 0.5:0.5:1 and dissolved in deionized water. The complexing agents, EDTA and citric acid, were added in sequence according to the mole ratio of EDTA to metal ions to citric acid, i.e., 1:1:2. The pH value of the solution was adjusted to ~6 by adding an appropriate amount of ammonia. The red-brown gel, obtained after heating of the solution under stirring for several hours over a hot plate, was fired at 250 °C and then calcined at 1000 °C for 5 h in air to obtain the final product. For the preparation of SDC, a stoichiometric amount of $Sm(NO_3)_3 \cdot 6H_2O$ and $Ce(NO_3)_3 \cdot 6H_2O$ were dissolved in deionized water under stirring. Ammonia was used to adjust the pH value to ~10. The brown suspension was transferred into an autoclave and then placed in an oven at 180 °C for 24 h. After being cooled to room temperature, the obtained precipitate was collected via suction filtration and washed with water 3 times and then dried. The precipitation was subsequently fired at 800 °C for 5 h in air to obtain the SDC powder.

### 2.2. Cathode ink preparation

The as-synthesized SSC and SDC powders were used for the preparation of the water-based cathode ink. The SSC and SDC powders were mixed at a weight ratio of 70:30 and dispersed in water. Then appropriate amounts of polyethylene glycol 4000 (PEG-4000) as a pore former and glycerine and polyacrylic acid as additives was added into the suspension. The detailed compositions are given in Table 1. After being milled at 400 rpm for 1 h in a high-energy ball miller (Model Pulverisette 6, Fritsch) and then treated for 30 min with an ultrasonic probe (Model JY92-11DN, Scientz Biotechnology), a well-dispersed cathode ink was finally obtained. To explore the effect of the pore former on the printed cathode layer, two inks with different contents of PVB were prepared.

### 2.3. Cell fabrication

An anode-supported thin film electrolyte cell configuration was adopted. The anode substrates were prepared using a tape-cast method. First, the anode slurry of NiO(Chengdu ShuduNano-Science Co. Ltd.) and YSZ (8 mol%, Tosoh) at a weight ratio of 6:4 with dimethylbenzene (Sinopharm Chemical Reagent Co. Ltd.) and ethanol as solvents and fish oil (Sigma–Aldrich) as a dispersant was ball milled for 24 h. Second, some organic additives and PVB binder were added to the slurry, followed by another ball milling for 24 h to obtain the final slurry. Then the slurry was casted on the tape at a speed of 5 m $min^{-1}$ and dried in air for 12 h. Disk-shaped pellets were punched and sintered at 1100 °C for 2 h to obtain the anode substrates. Next, a thin-film YSZ electrolyte layer and SDC buffering layer in sequence were deposited onto one surface of the anode substrate via a wet powder spraying technique. The prepared half-cells were then co-fired at 1400 °C for 2 h in air to obtain the inkjet printing triple-layered substrate.

In the study, a modified HP Deskjet 2668 printer and black ink cartridge (HP CC640ZZ 818) were used as the printing unit and the ink container, respectively, with a printing resolution of 600 dpi. The inks were filled into cartridges using syringes. The printing speed was kept constant for the whole printing process. Typically, 20 s was required to produce a total surface area of 100 $cm^2$ for each printing. A total of 45 passes of the cathode were printed over the triple-layered substrate in a similar manner.

**Table 1**
Ink formulations used for inkjet printing.

| Constituent | SSC/SDC | $H_2O$ | PEG-4000 | PAA | Glycerine |
|---|---|---|---|---|---|
| Quantity (g) | 2 | 36.2 | 1 | 0.3 | 0.5 |

### 2.4. Basic characterization

The phase structure of the synthesized powder was analyzed by X-ray diffraction (XRD, BrukerD8 Advance) at room temperature. Environmental scanning electron microscopy (ESEM, FEI Company, Quanta-2000) was used to identify the morphologies of the fabricated cells. The elemental distribution on the cross-section of the electrode layers were analyzed using a field-emission scanning electron microscopy (FESEM, Hitachi S-4800) equipped with an energy-dispersive X-ray analyzer (EDX). The particle size distribution of the ink was measured using a laser particle size analyzer (LPSA, Microtrac S3500). The viscosity of the ink was measured using an in-lab rotational viscometer. The surface tension was measured with a tensiometer (KSV Sigma-70).

### 2.5. Cell performance test

The electrochemical performance of the single cell was performed in an in-lab constructed station. The cell was sealed onto the top of a quartz with the anode side flowing with fuel gas, whereas the cathode side was exposed to ambient atmosphere. During the testing process, the furnace was heated to the desired temperature at a heating rate of 10 °C $min^{-1}$. Hydrogen was introduced into the anode side at a flow rate of 20 ml $min^{-1}$ [STP] to reduce NiO for 1–2 h, then the flow rate of hydrogen was increased to 80 ml $min^{-1}$. *I–V* curves were obtained using a Keithley 2420 digital source meter in the four-probe mode. Electrochemical impedance spectra (EIS) ware measured with a Solartron 1260A frequency-response analyzer in combination with a Solartron 1287 potentiostat. The Frequencies used for the EIS measurements ranged from 10 kHz to 0.1 Hz with a signal amplitude of 10 mV under open-circuit conditions.

## 3. Results and discussion

### 3.1. Properties of cathode powder and ink

A stable ink is a key point toward the successful preparation of a thin-film layer by inkjet printing. In addition, a low viscosity of the ink is required when applying the commercial HP inkjet printer (HP Deskjet 2668) as the apparatus for film preparation. Considering the high theoretical density of SSC ($6.83 \times 10^3$ kg $m^{-3}$) and SDC ($7.15 \times 10^3$ kg $m^{-3}$), as a comparison of $1.0 \times 10^3$ kg $m^{-3}$ for water, and the low viscosity of water ($0.8937 \times 10^{-3}$ N s $m^{-2}$), the particle sizes of the powders should be as small as possible to avoid the sediment of the oxide powders by gravimetric effect. The particle size of a powder is highly dependent on the synthesis method and the sintering temperature. The solid-state reaction was widely applied for the synthesis of ceramic materials, which requires a high calcination temperature to overcome the diffusion block for reactants, producing oxide powders with large grain size. In this study, the EDTA-CA complexing method was used for the synthesis of SSC, while the SDC powder was synthesized using a hydrothermal process [43]. Both methods can allow the mixing of raw materials at molecular levels, thus ensuring the synthesis of a phase-pure composite oxide at low temperatures. Because calcination at high temperature often promotes grain growth, a lower calcination temperature could result in finer particle size. It should be noted that the high phase purity is very important to achieve high electrochemical performance of the oxides because both the oxygen surface exchange kinetics and bulk diffusion properties of the oxides are closely related to their phase structures. Fig. 1 shows the corresponding XRD patterns of the synthesized powders. After the calcination at 1000 °C and 800 °C, respectively for SSC and SDC, phase-pure oxides were obtained. The SDC displayed a typical

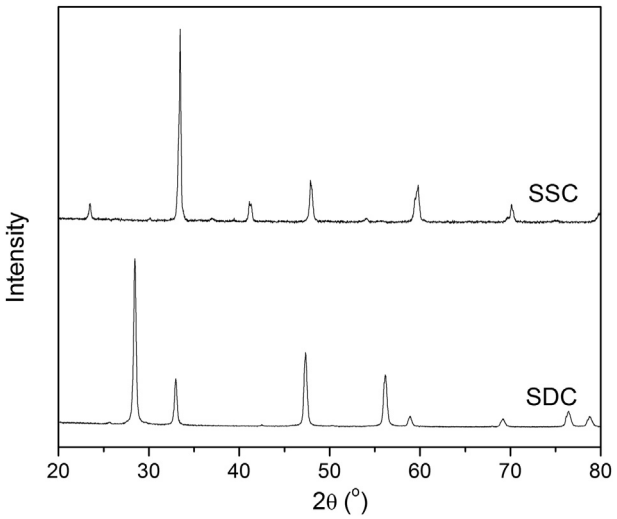


**Fig. 1.** X-ray diffraction patterns of the synthesized SSC and SDC powders.

fluorite phase structure with cubic lattice symmetry, and the SSC displayed a fully crystallized perovskite-type lattice structure. The lattice parameters of the SSC and SDC, obtained by Rietveld refinement of the XRD patterns, were observed to be $a = 5.398(6)$ Å, $b = 7.574(7)$ Å, $c = 5.357(4)$ Å ($R_{wp} = 5.94\%$, $R_p = 4.74\%$, CHI**2 = 1.712) and $a = 5.436(1)$ Å ($R_{wp} = 5.95\%$, $R_p = 4.9\%$, CHI**2 = 1.647), respectively, which matched well with SSC (ICSD: 00-053-0112) and SDC (ICSD: 01-075-0158).

As-synthesized powders from the wet chemical method may still contain a certain level of soft aggregation. To prepare a stable ink suspension of the composite electrode materials (SSC + SDC) with small particle size, an appropriate amount of SSC and SDC powders were mixed by hand and further ball-milled together with PEG-400 in de-ionized water for 1 h and then ultrasonically dispersed for 30 min. In Fig. 2, the particle size distributions of the oxides in the ink are shown, as measured with a laser particle size analyzer. Most of the particle sizes ranged from 0.5 to 7 μm, and two particle size distribution peaks, 0.8 and 2 μm, were observed with weight percentages of 10.5 and 14%, respectively. Notably, the larger size particles corresponding to the second distribution peak

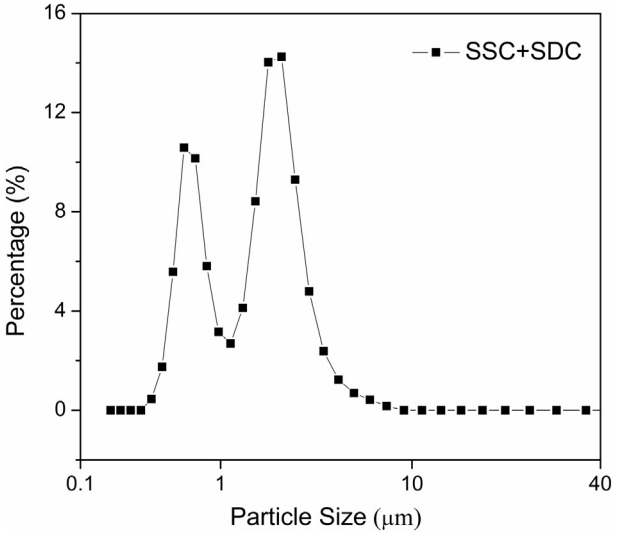


**Fig. 2.** Particle size distribution of the SDC/SSC ink.

in this study were smaller than those of the previous YSZ (5.5 μm) and SDC (7.8 μm) for the electrolyte layer prepared by a similar process [38]. This finding suggests that the soft aggregation in the oxide powders was successfully broken down after conducting the ball milling process.

To examine the stability of the as-prepared ink, it was subjected to aging at room temperature for a period of 3 days. As observed in Fig. 3, after the aging, no sedimentation appeared. This finding suggests that after the ball milling process, the oxide powders were sufficiently small that the van der Waals force successfully overcame the effect of gravity of the powder.

A dimensionless number $Z$, the inverse of the Ohnesorge (Oh), is usually used to determine the printability of ink [44,45]:

$$\mathrm{Oh} = \frac{\eta}{\sqrt{\sigma\rho\alpha}}, \quad (1)$$

where $\eta$ is the viscosity of the ink, $\sigma$ is the surface tension, $\rho$ is the density, and $\alpha$ is a characteristic length.

The $Z$ value is related to the density, viscosity and surface tension of the ink. Derby et al. determined that the $Z$ value for printable inks should be between 1 and 10, whereas Jang et al. redefined the printable range as $4 \leq Z \leq 14$ [46,47]. In this study, the $Z$ value of the ink was calculated to be 4.54 according to Eq. (1) and the measured ink properties (Table 2), which indicates that the ink is feasible for inkjet printing.

For the fabrication of a thin film layer by inkjet printing, the oxide powder in the ink usually has an ultrafine particle size, as demonstrated by the laser particle size distribution analysis presented previously; thus, it is very easily sintered at elevated temperature. To achieve sufficient porosity for a cathode prepared by inkjet printing, some pore former was introduced into the ink in this study. However, during the burning out of the pore former, abundant $CO_2$ was released, which may react with strontium ions in the SSC to form an impurity phase (bulk or surface carbonate). Such impurity phases usually exhibit poor electrochemical activity for the oxygen reduction reaction and thus should be avoided. However, co-sintering of the electrode with the electrolyte layer as an appropriate temperature is required to create sufficient strength of the electrode layer and firm adhesion of the electrode layer to the electrolyte layer. Typically, a firing temperature of 1000 °C is applied [48]. Fig. 4 presents the XRD patterns of the electrode layer after the calcination in air at 1000 °C for 2 h, prepared by ink printing with the presence of a pore former. The diffraction peaks of the SSC + SDC composite electrode can be well indexed based on the physical mixture of the SSC phase and SDC phases, and no other impurity phase such as carbonate was observed. This finding suggests a calcination of 1000 °C is sufficient to avoid the formation of an impurity phase during the burning out of the pore former.

**Table 2**
Ink properties and dimensionless value of SSC/SDC ink.

| Ink properties | $\rho$ (g cm$^{-3}$) | $\sigma$ (m Nm$^{-1}$) | $\eta$ (m Pas) | $Z$ |
|---|---|---|---|---|
| SSC/SDC | 1.05 | 71.50 | 8.74 | 4.54 |

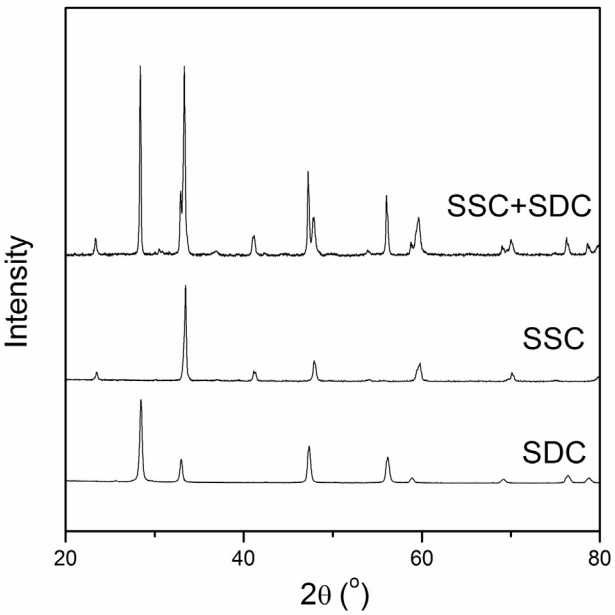


**Fig. 4.** X-ray diffraction patterns of the powder with the ink post calcination.

### 3.2. Morphological structure of the cathodes

To explore the effect of the pore former in the ink on the printed cathode performance, three different SSC + SDC composite electrodes were fabricated by inkjet printing without the adoption of a pore former and with 15% and 10% PVP-K30 pore formers and the related electrodes were labeled electrode-01, electrode-02 and electrode-03, respectively. As observed in Fig. 5, after the sintering

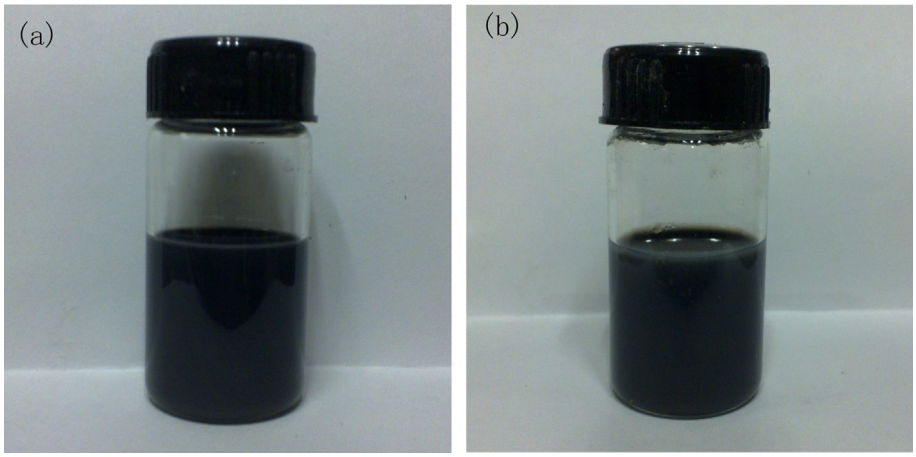


**Fig. 3.** Digital photographs of SC/SDC inks, (a) fresh ink, and (b) the ink after aging for 3 days.

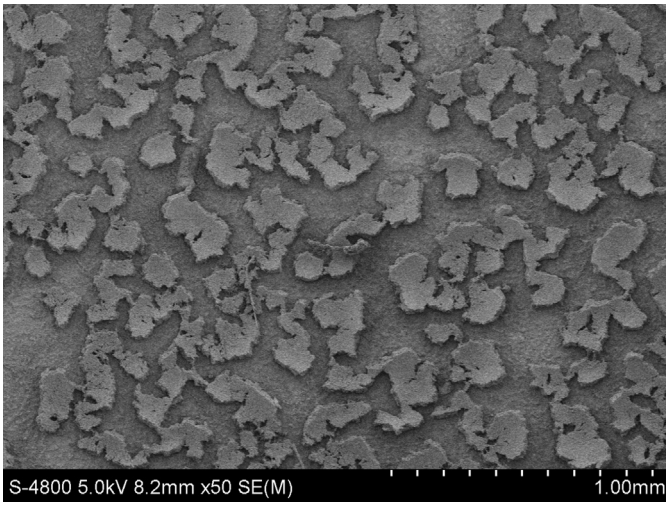


**Fig. 5.** Representative SEM image of the cathode layer as fabricated by inkjet-printing with the ink containing 15% PVP pore former.

at high temperature to remove the organic additive, the electrode layer of electrode-02 did not form a continuous network over the electrolyte (SDC) surface; the electrode layer instead contained isolated islands. This finding suggests an appropriate amount of the pore former is vital to achieve a cathode layer with good geometric integrity for the electrode prepared by inkjet printing.

Fig. 6 presents cross-sectional SEM images of electrode-01 and electrode-03; for comparison, an electrode prepared by conventional spray deposition was also prepared. For the electrode prepared by spray deposition, good geometric integrity and high porosity were observed (Fig. 6a). As expected, for the electrode layer prepared without the adoption of a pore former, because of the easy sintering of the ultrafine electrode powder, the material was badly sintered with few pores, which could limit the gas transportation and reduce the number of active sites for the oxygen reduction reaction (Fig. 6b). For the electrode prepared by inkjet printing with 10 wt.% pore former in the ink (electrode-03), the electrode exhibited a highly porous microstructure and a homogeneous thickness of approximately 12–15 μm, which was adhered firmly onto the SDC buffer layer (Fig. 6c). The electrode particles were well connected to each other and formed a continuous path for electron conduction.

### 3.3. Electrochemical performance

The single cells with the SSC + SDC composite cathode, fabricated using inkjet printing, were then subjected to electrochemical performance tests. The effect of the pore former in the cathode ink on the electrochemical performance was specifically investigated. For comparison, a similar cell with a SSC + SDC composite cathode, prepared using a conventional spray deposition method, was also tested. For all three cells under investigation in this section, their electrolyte and anode were kept as similar as possible, including the thickness, porosity (anode) and composition, by selecting all the anode-supported thin film electrolyte dual layer cells from the same batch of fabrication.

Fig. 7 presents the *I*–*V* curves at the temperature range of 550–750 °C of the cell with the spray-deposition-derived cathode

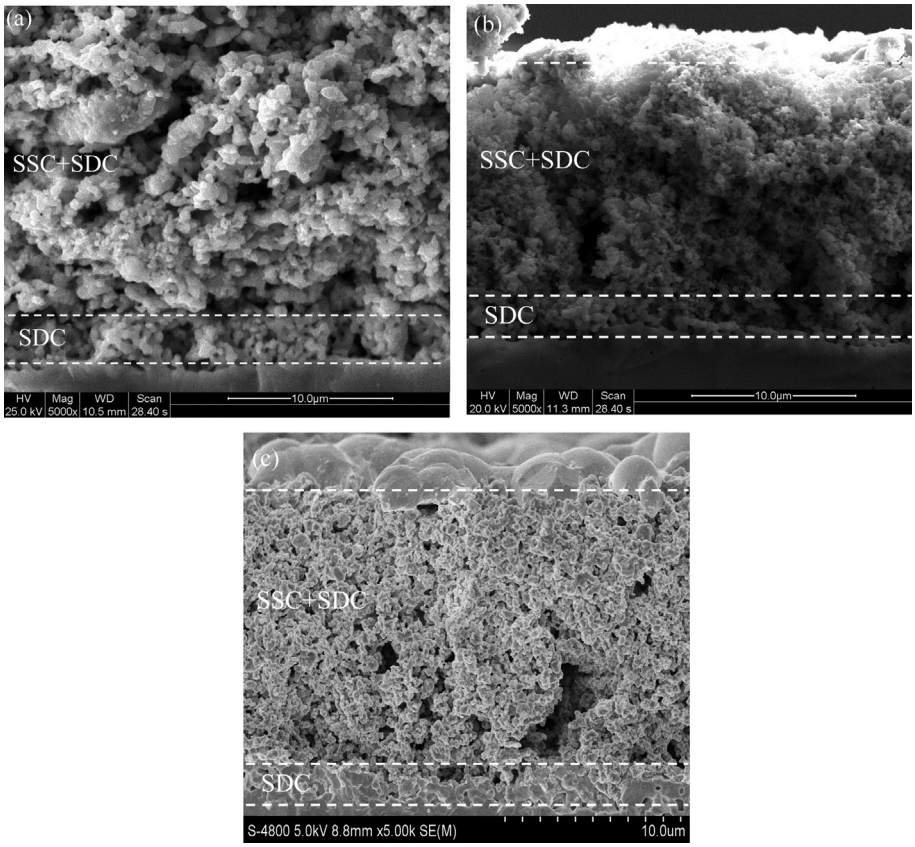


**Fig. 6.** SEM images from cross-sectional view of the cathode layer, (a) an electrode prepared by conventional spray method, (b) electrode-01 without the adoption of a pore former and (c) electrode-03 containing 10% PVP-K30.

(cell-01), the cell with the inkjet-printed cathode without the pore former (cell-02), and the cell with the inkjet-printed cathode with 10 wt.% pore former in the cathode ink (cell-03). For all three cells, high OCVs of approximately 1.10 V were achieved at all the investigated temperatures, which are near the theoretical values, indicating that all the electrolytes were well densified and that the electrode exhibited favorable electrochemical activity. For cell-01 with the conventional spray deposition cathode, maximum power densities of 1150, 750, 450, 250 and 120 mW $cm^{-2}$ were reached at 750, 700, 650, 600 and 550 °C, respectively. In comparison, for cell-02 with the electrode prepared by inkjet printing without the adoption of the pore former in the ink, much poorer cell performance was observed. For example, the peak power densities were only 550, 350, 200, 100 and 45 mW $cm^{-2}$ at 750, 700, 650, 600 and 550 °C, respectively. This difference in cell performance was clearly mainly due to the cathode. Notably, a linear response of the cell voltage to polarization current was still demonstrated for cell-02, even at high current density. This finding suggests that no serious concentration polarization occurred in the cathode of cell-02, although the poor sintering of the cathode is clearly observed in Fig. 6b. Thus, the reduced length of the triple phase boundary due to the sintering of the cathode very likely contributed to the poor performance of cell-02. By applying pore former (10 wt.%) in the cathode ink for inkjet printing, significant cell performance improvement was observed. As observed in Fig. 7c, peak power densities of 950, 620, 370, 150 and 100 mW $cm^{-2}$ were obtained for cell-03 at 750, 700, 650, 600 and 550 °C, respectively, which represent an approximately 80% improvement compared with those of cell-02. Similarly, no concentration polarization was observed for cell-03. The significant improvement in cell power output by applying the pore former in the cathode ink clearly was closely related to the increased electrode porosity.

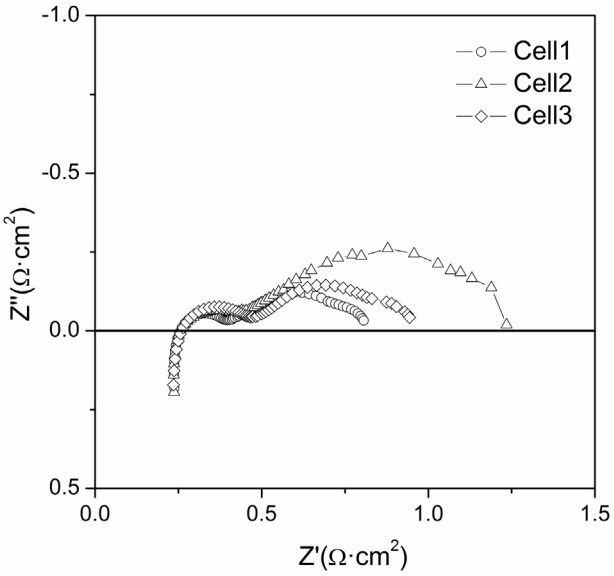


**Fig. 8.** EIS of the three cells at 750 °C.

To further demonstrate the improved cell performance, the three cells were further measured by EIS. In Fig. 8, the EIS spectra at 750 °C under open-circuit conditions are presented. The ohmic

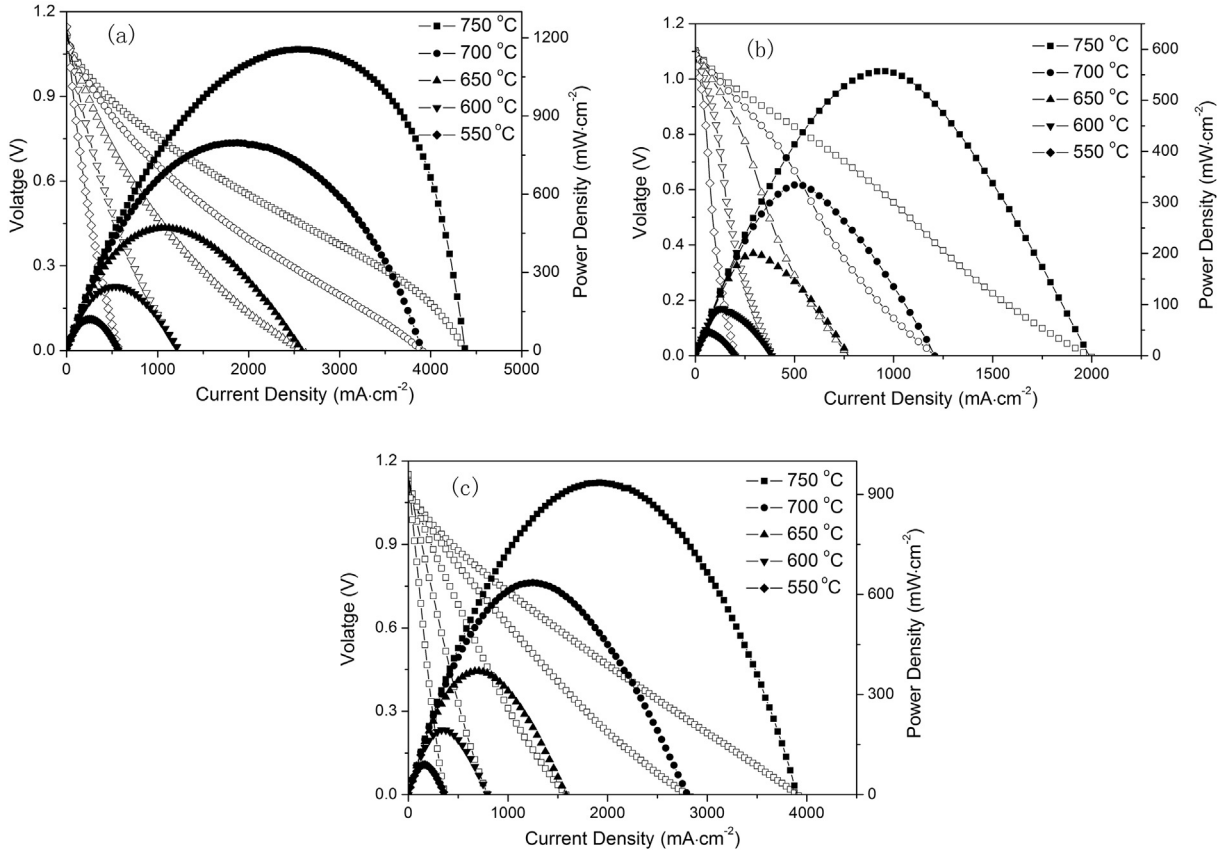


**Fig. 7.** *I–V* and *I–P* polarization curves of the three cells (a) Cell-01: with the cathode by wetting powder spraying (b) Cell-02: with the cathode without pore former (c) Cell-03: with the cathode containing 10% PVP-K3.

resistance ($R_s$) of each cell corresponds to the intercept of the impedance curve with the real axis at the high frequency side, which was mainly derived from the ohmic resistance of the YSZ electrolyte layer and the buffering layer. The difference of the impedance *arc* with the real axis corresponds to the polarization resistance ($R_p$) of the cell, which is correlated to electrode processing, and both the anode and cathode contributed to the resistance. Because the anodes and electrolytes were prepared in the same manner, the main difference in the performance of the three cells was due to the cathode side. According to the EIS spectra presented in Fig. 8, two depressed arcs were observed. Only considering the cathode, Kim et al. suggested that the high-frequency arc could be correlated with oxygen ion transfer from the TPB to the electrolyte and should be related to the length of the TPB, while the low-frequency *arc* was correlated with the diffusion of $O^-$ species along the cathode surface to the TPB and the diffusion of oxygen molecules in electrode pores [49]. This finding suggests that the resistance of the low-frequency arc in this study was related to the length of TPB as well as the porosity of the cathode. For all three cells, the $R_s$ values were similar to each other, i.e., approximately 0.22 Ω $cm^2$, which suggests that the experimental processes exhibit good reproducibility. However, the low-frequency *arc* values, greatly varied with values of 0.4 Ω $cm^2$, 0.8 Ω $cm^2$ and 0.5 Ω $cm^2$ for cell-01, cell-02 and cell-03, respectively. The large *arc* of cell-02 may be related to the low porosity of the cathode from poor sintering, which significantly decreased the effective TPB for the electrochemical reduction of oxygen. Cell-03 with a pore former in the cathode ink had a much smaller arc than that of cell-02 and exhibited a comparable resistance to cell-01. These findings thus further proved the importance of the cathode porosity on the performance of electrode.

## 4. Conclusions

In this work, a SDC/SSC composite cathode layer was successfully fabricated using an inkjet printing technique using environmentally friendly water-based ink. A well-dispersed suspension using the optimized powder synthesis method was prepared for inkjet printing. As the thin film layer prepared by inkjet was easy to sinter and formed a dense cathode, a pore former was added to increase the diffusion of oxygen molecules. The addition of the pore former in the ink greatly improved the cell electrochemical performance, with a PPD as high as 940 mW $cm^{-2}$ at 750 °C, which was comparable to that of the cell prepared using the conventional wet powder spraying method. This study further demonstrates that the inkjet printing technique is highly attractive and practical for SOFC fabrication.

## Acknowledgments

This study was supported by an ARC future fellowship under contract no. FT100100134. Prof. Huili Chen would also like to thank Curtin University for a visiting scholarship.

## References

[1] K. Huang, J.B. Goodenough, Solid Oxide Fuel Cell Technology: Principles, Performance and Operations, first ed., Woodhead Publishing in Energy, 2009, pp. 141–154 (Chapter 8).
[2] Q.H. Liu, Y. Tian, H.J. Li, L.J. Jia, C. Xia, L.T. Thompson, Y.D. Li, J. Power Sources 195 (2010) 6539–6548.
[3] M.W. Ellis, M.R. VonSpakovsky, D.J. Nelson, Proc. IEEE 89 (2001) 1808–1818.
[4] T.M. Gur, Chem. Rev. 113 (2013) 6179–6206.
[5] J. Lin, C.W. Babbitt, T.A. Trabold, Bioresour. Technol. 128 (2013) 495–504.
[6] H.C. Patel, T. Woudstra, P.V. Aravind, Fuel Cells 12 (2012) 1115–1128.
[7] E. Facchinetti, M. Gassner, M. D'Amelio, F. Marechal, D. Favrat, Energy 41 (2012) 408–419.
[8] M.L. Li, M. Ni, F. Su, C.R. Xia, J. Power Sources 260 (2014) 197–204.
[9] J.G. Lee, M.G. Park, S.H. Hyun, Y.G. Shul, Electrochim. Acta 129 (2014) 100–106.
[10] S.C. He, R.F. Li, L. Ge, H. Chen, L.C. Guo, J. Alloys Compd. 576 (2013) 242–246.
[11] F.C. Wang, D.J. Chen, Z.P. Shao, Electrochim. Acta 103 (2013) 23–31.
[12] M.A. Nath, A.S. Hameed, R. Chockalingam, S. Basu, A.K. Ganguli, Fuel Cells 13 (2013) 270–278.
[13] L. Guo, J.M. Calo, E. DiCocco, E.J. Bain, Energy Fuels 27 (2013) 1772–1778.
[14] P. Kalra, R. Garg, A. Kumar, Mater. Sci. Forum: Eng. Appl. Nanosci. Nanomater. 757 (2013) 217–241.
[15] D.J. Chen, C. Chen, F.F. Dong, Z.P. Shao, F. Ciucci, J. Power Sources 250 (2014) 188–195.
[16] F.F. Dong, Y.B. Chen, R. Ran, D.J. Chen, M.O. Tade, S.M. Liu, Z.P. Shao, J. Mater. Chem. A 1 (2013) 9781–9791.
[17] J. An, Y.B. Kim, J. Park, T.M. Gur, F.B. Prinz, Nano Lett. 13 (2013) 4551–4555.
[18] Y.B. Kim, T.P. Holme, T.M. Gur, F.B. Prinz, Adv. Funct. Mater. 21 (2011) 4684–4690.
[19] D.J. Chen, R. Ran, K. Zhang, J. Wang, Z.P. Shao, J. Power Sources 188 (2009) 96–105.
[20] J.H. Shim, S. Kang, S.W. Cha, W. Lee, Y.B. Kim, J.S. Park, T.M. Gur, F.B. Prinz, C.C. Chao, J.W. An, J. Mater. Chem. A 1 (2013) 12695–12705.
[21] M. Haydn, K. Ortner, T. Franco, S. Uhlenbruck, N.H. Menzler, D. Stover, G. Brauer, A. Venskutonis, L.S. Sigl, H.P. Buchkremer, R. Vassen, J. Power Sources 256 (2014) 52–60.
[22] H.S. Noh, K.J. Yoon, B.K. Kim, H.J. Je, H.W. Lee, J.H. Lee, J.W. Son, J. Power Sources 247 (2014) 105–109.
[23] J. Qian, Z.W. Zhu, J.J. Dang, G.S. Jiang, W. Liu, Electrochim. Acta 92 (2013) 243–247.
[24] Z.R. Wang, J.Q. Qian, H.D. Cao, S.R. Wang, T.L. Wen, J. Alloys Compd. 437 (2007) 264–268.
[25] C. Fu, X. Ge, S.H. Chan, Q. Liu, Fuel Cells 12 (2012) 450–456.
[26] N.H. Menzler, J. Malzbender, P. Schoderböck, R. Kauert, H.P. Buchkremer, Fuel Cells 14 (2014) 96–106.
[27] R.C. Pullar, Y. Zhang, L.F. Chen, S.F. Yang, J.R.G. Evans, P.K. Petrov, A.N. Salak, D.A. Kiselev, A.L. Kholkin, V.M. Fereira, N.M. Alford, J. Eur. Ceram. Soc. 27 (2007) 4437–4443.
[28] T.M. Wang, B. Derby, J. Am. Ceram. Soc. 88 (2005) 2053–2058.
[29] X. Zhao, J.R.G. Evans, M.J. Edirisinghe, J.H. Song, J. Mater. Sci. 37 (2002) 1987–1992.
[30] C. Ainsley, N. Reis, B. Derby, J. Mater. Sci. 37 (2002) 3155–3161.
[31] M. Mott, J.R.G. Evans, Mater. Sci. Eng. A 271 (1999) 344–352.
[32] T. Kawase, S. Moriya, C.J. Newsome, T. Shimoda, Jpn. J. Appl. Phys. 44 (2005) A3649–A3658.
[33] T. Xu, S. Petridou, E.H. Lee, E.A. Roth, N.R. Vyavahare, J.J. Hickman, T. Boland, Biotechnol. Bioeng. 85 (2004) 29–33.
[34] A.M. El-Toni, T. Yamaguchi, S. Shimizu, Y. Fujishiro, M. Awano, J. Am. Ceram. Soc. 91 (2008) 346–349.
[35] D. Young, A.M. Sukeshini, R. Cummins, H. Xiao, M. Rottmayer, T. Reitz, J. Power Sources 184 (2008) 191–196.
[36] C.F. Wang, S.C. Hopkins, R.I. Tomov, R.V. Kumar, B.A. Glowacki, J. Eur. Ceram. Soc. 32 (2012) 2317–2324.
[37] R.I. Tomov, M. Krauz, J. Jewulski, S.C. Hopkins, J.R. Kluczowski, D.M. Glowacka, B.A. Glowacki, J. Power Sources 195 (2010) 7160–7167.
[38] C. Li, H.G. Shi, R. Ran, C. Su, Z.P. Shao, Int. J. Hydrogen Energy 38 (2013) 9310–9319.
[39] C.F. Wang, R.I. Tomov, R.V. Kumar, B.A. Glowacki, J. Mater. Sci. 46 (2011) 6889–6896.
[40] A.M. Sukeshini, R. Cummins, T.L. Reitz, R.M. Miller, Electrochem. Solid State Lett. 12 (2009) B176–B179.
[41] N. Yashiro, T. Usui, K. Kikuta, J. Eur. Ceram. Soc. 30 (2010) 2093–2098.
[42] M. Dudek, R.I. Tomov, C. Wang, B.A. Glowacki, P. Tomczyk, R.P. Socha, M. Mosialek, Electrochim. Acta 105 (2013) 412–418.
[43] H.G. Shi, W. Zhou, R. Ran, Z.P. Shao, J. Power Sources 195 (2010) 393–401.
[44] B. Derby, Annu. Rev. Mater. Res. 40 (2010) 395–414.
[45] E. Özkol, J. Ebert, R. Telle, J. Eur. Ceram. Soc. 30 (2010) 1669–1678.
[46] B. Derby, N. Reis, MRS Bull. 28 (2003) 815–818.
[47] D. Jang, D. Kim, J. Moon, Langmuir 25 (2009) 2629–2635.
[48] X.G. Zhang, M. Robertson, S. Yick, C. Dêces-Petit, E. Styles, W. Qu, Y.S. Xie, R. Hui, J. Roller, O. Kesler, R. Maric, D. Ghosh, J. Power Sources 160 (2006) 1211–1216.
[49] J.D. Kim, G.D. Kim, J.W. Moon, Y.I. Park, W.H. Lee, K. Kobayashi, M. Nagai, C.E. Kim, Solid State Ionics 143 (2001) 379–389.